 doi:10.20944/preprints202208.0334.v1

Article

Split Ring Resonator Network and Diffused Sensing Element Embedded in a Concrete Beam for Structural Health Monitoring

Erika Pittella*,[1], Raissa Schiavoni[2], Giuseppina Monti[2], Antonio Masciullo[2], Marco Scarpetta[3], Andrea Cataldo*,[2] Emanuele Piuzzi[1]

[1] Department of Information Engineering, Electronics and Telecommunications (DIET) Sapienza - University of Rome, Roma, Italy;
[2] University of Salento-Department of Engineering for Innovation, Complesso Ecotekne - Corpo O, 73100 Lecce, Italy;
[3] Department of Electrical and Information Engineering, Politecnico di Bari, Via E. Orabona 4, 70125 Bari, Italy;
* Correspondence: erika.pittella@uniroma1.it (E.P.); andrea.cataldo@unisalento.it (A.C.)

Abstract: The aim of this work is to propose two different and integrated sensors for the structural health monitoring of concrete beams. In particular, a diffused sensing element and a split ring resonator network are presented. The first sensor is able to detect the variation of the dielectric properties of the concrete along the whole beam length, for a diffuse monitoring both during the important concrete curing phase and also for the entire life cycle of the concrete beams. The resonators instead work punctually, in their surroundings, allowing an accurate evaluation of the permittivity both during the drying phase and after. This allows the continuous monitoring of any presence of water both inside the concrete beam and in points that can be critical, in the case of beams in dams, bridges or in any case subject to a strong presence of water which could lead to deterioration, or worse, cause serious accidents. Moreover, the punctual sensors are able to detect the presence of cracks in the structure and to localize them.

Keywords: structural health monitoring; sensing element; split ring resonator; continuous monitoring; sensor network

1. Introduction

Civil infrastructure systems such as bridges, buildings, dams, and pipelines play a central role for the economic and industrial wealth of society [1]. Monitoring health conditions of above-mentioned infrastructures, often exposed to various external loads and problematic environmental conditions, is of crucial importance to avoid failures and for planning maintenance actions [2]. For these reasons Structural Health Monitoring (SHM), that includes the integration of sensors, smart materials, data transmission, computational power, and processing ability integrated within the structures [3], is currently one of the leading research topics of structural engineering [4].

The most widely used construction material in the world is the concrete, thanks to its strength, durability, versatility, and cost effectiveness. Concrete is a mixture of Portland cement, water, aggregates, and in some cases, admixtures; its properties depend on the relative amounts and characteristics of the individual components. Even a perfect mix can result in poor quality concrete if the curing phase is not properly monitored [5]. The concrete hardening phase period is considered completed within the first 28 days (with the first 48 hours being the most critical) during which an accurate monitoring is actually of vital importance [6].

Indeed, a premature removal of formworks may lead to an inadequate structure strength and to the presence of cracks, produced by internal possible strain, that can cause

 doi:10.20944/preprints202208.0334.v1

the collapse of the structure at a later time. Moreover, the ex-post monitoring has also a great importance, since it allows an immediate response in case of anomalies, decay phenomena, and also in the case of structures in contact with water such as dams, river banks etc.

Recently, the monitoring of moisture content in concrete structures and their consequent deterioration has triggered the interest in electromagnetic sensors [7]-[10].

In particular, in [10] the design of a split ring resonator (SRR) network, composed of sensors with different resonance frequencies to both monitor and localize possible cracks, is proposed. Preliminary experimental results have shown that the sensors can monitor a concrete crack of few millimeters. These sensors can offer an accurate but relatively confined monitoring of the structure; therefore, the combination with a wire-like diffused sensing element [11] can be a winning solution in order to monitor the structure along the entire length, for detecting dielectric variation both during the curing process and for the entire useful life of the structure.

On the bases of the results presented in [10], the number of SRRs has been extended and the network has been designed, fabricated and tested in a realistic scenario, namely integrated in a concrete beam together with a wire-like diffused sensing element. Both sensors can be permanently embedded in buildings, structures, infrastructures at the time of construction, returning a response based on material dielectric characteristics, particularly useful for early identification of destructive phenomena.

The present work is organized as follows. Section 2 presents the SRR network design and the diffused sensing element. Section 3 describes the experimental set-up. Experimental results are reported in Section 4. Finally, conclusions and the future developments are outlined in Section 5.

2. Split Ring Resonator Network Design

2.1. SRR Network

An SRR is made up of metal tracks on a dielectric substrate; these tracks consist of circular crowns with cuts along a diameter, hence the name “Split Ring” resonator. There are various types of SRR which differ in geometry [12]. Starting from microwave applications of SRR [13], [14], we have focalized on SRRs used for material dielectric characterization [15]-[17] and, in particular, SRRs with high sensitivity, high quality factor, small size, and that do not require a particular sample preparation [13], [18]. As detailed in [10] the choice of the substrate depends on resonator requirements in terms of quality factor, possible dispersion effects, and other practical needs as well as availability on the market.

In particular, the substrate thickness affects both the losses and the practical needs for measurement. For this latter, it is obvious that the greater the thickness, the greater the strength of the resonator leading to a good repeatability of the measurements and, especially, to a high accuracy. To determine the suitable substrate and to optimize the geometric parameters of the SRR with reference to the desired resonance frequency and optimal quality factor, parametric simulations were performed with EM CAD CST Microwave Studio [19], using various substrates available on the market and obtaining the scattering parameter matrix for each SRR. These optimization simulations were performed with the SRR in air, employing perfectly matched layer (PML) absorbing boundary conditions, and the datasheet specifications for the substrate material properties. From the analysis of the transmission coefficient and the quality factor, the AD255C material from Rogers Corporation with thickness 0.040” (1.016 mm) was chosen, with $\varepsilon_r = 2.55$; loss tangent = 0.0013 @10 GHz; t = 0.035 mm, where t is the thickness of the copper cladding [20].

Four similar SRRs have been designed and optimized, using the same material and varying the geometric characteristics (their principal parameters are displayed in Fig. 1) to achieve different resonance frequencies. In this way, a network to be used to monitor

Preprints (www.preprints.org) | NOT PEER-REVIEWED | Posted: 18 August 2022 doi:10.20944/preprints202208.0334.v1

concrete structures can be implemented, in order to detect changes in the dielectric properties of the material under test and/or to identify the presence of possible cracks in the vicinity of the sensitive elements.

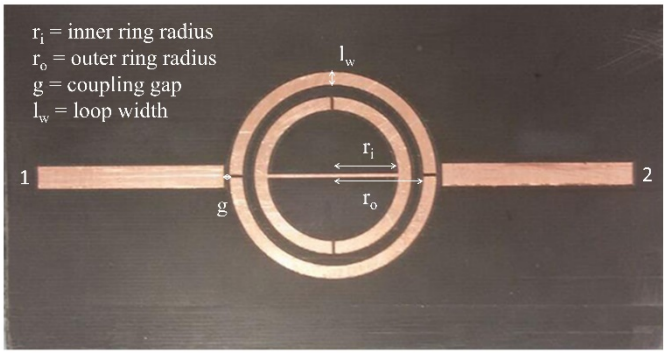

Figure 1. Split ring resonator geometry and its principal parameters.

Table 1 shows the geometrical characteristics for the 4 SRRs and Fig. 2 shows the corresponding transmission coefficients (scattering parameter S_{21}) for the four sensors operating in air.

Subsequently, the SRRs have been simulated with the numerical CAD, embedded in a medium with a permittivity ε that has been varied from 1 to 8, with step 1. Figure 3 shows the relationship between the resonance frequency f_r and the permittivity ε for the SRR1, while Table 2 contains simulation results for all four SRRs.

Table 1. Geometric dimensions of Split Ring Resonators.

SRR	r_i (mm)	r_o (mm)	g (mm)	l_w (mm)
1	14.0	18.0	0.44	2.0
2	12.4	16.4	0.44	2.0
3	11.0	15.0	0.44	2.0
4	10.0	14.0	0.44	2.0

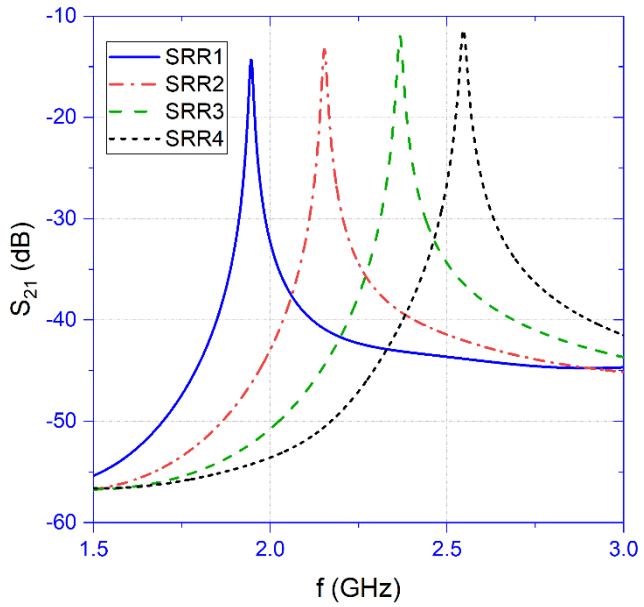

Figure 2. Transmission coefficients of split ring resonators in air.

Preprints (www.preprints.org) | NOT PEER-REVIEWED | Posted: 18 August 2022 doi:10.20944/preprints202208.0334.v1

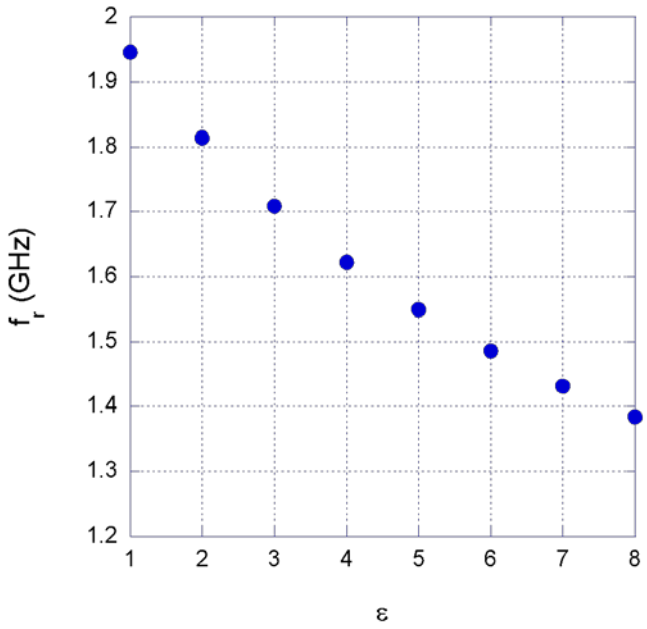

Figure 3. Relationship between the SRR1 resonance frequency and the permittivity of the surrounding material.

Table 2. Resonance frequency of the four split ring resonators embedded in a material with permittivity ε.

ε	1	2	3	4	5	6	7	8
$f_{r,SRR1}$	1.9461	1.8141	1.7082	1.6224	1.5489	1.4856	1.4313	1.3842
$f_{r,SRR1}$	2.1531	2.0091	1.8894	1.7910	1.7109	1.6407	1.5771	1.5222
$f_{r,SRR3}$	2.3670	2.2101	2.0772	1.9710	1.8819	1.8039	1.7364	1.6737
$f_{r,SRR4}$	2.5464	2.3733	2.2347	2.1231	2.0268	1.9431	1.8690	1.8015

2.2. Power Divider

In order to feed the four SRRs, the design of a power divider has been conducted with Microwave Office (MWO) by AWR [21]. In particular, a resistive power divider is considered since it is the simplest circuit topology, the smallest, and the most broadband; on the other hand, it also has high losses.

Figure 4 shows a schematic of the network: the presence of identical 16×2/3 Ω resistors insures that the divider does present an input impedance of 50 Ω at all the ports [22]. The substrate used for the circuit design is the Rogers RO4003, whose principal characteristics are contained in Fig. 4. The same scheme has been adopted for the combiner, that is used at the SRRs output to combine the four-feed lines into a single one, to allow transmission coefficient measurements of the entire network. The MWO simulation results for the divider/combiner network highlight an insertion loss ranging from 10 to 15 dB within the SRR operating frequency band. The scattering parameters of the single SRRs obtained through the CST full-wave simulations have been used for implementing the entire sensor network within MWO software, thus obtaining the S_{21} of the entire sensor network.

Figure 5 shows the S_{21} of the entire sensor network (port 1 and 2 are the input port and the output port shown in Fig. 4, respectively) in the case of SRRs embedded in a material equal to air, i.e. with ε = 1. The simulation shows 4 peaks in the S_{21} response of the entire network which, as expected, correspond to the resonance peaks of the four SRRs previously designed. Comparing Fig. 2, which refers to the single SRRs in air, and Fig. 5,

Preprints (www.preprints.org) | NOT PEER-REVIEWED | Posted: 18 August 2022 doi:10.20944/preprints202208.0334.v1

which refers to the entire network in similar conditions, a decrease of 20 to 30 dB in transmission can be observed, which is due to the previously highlighted insertion losses of the power splitter and combiner.

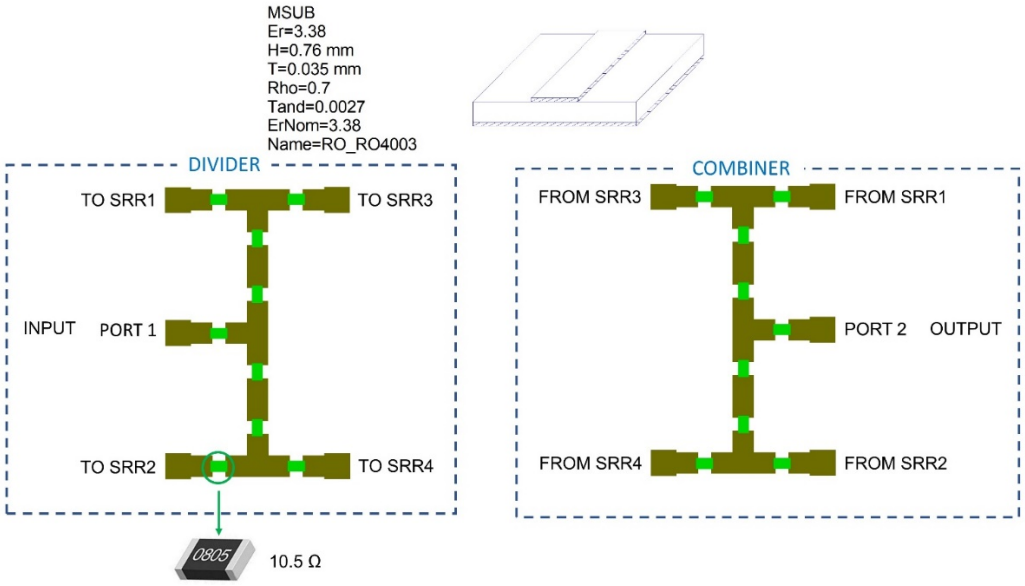

Figure 4. Scheme of the network with the MWO schematic of the power divider and combiner.

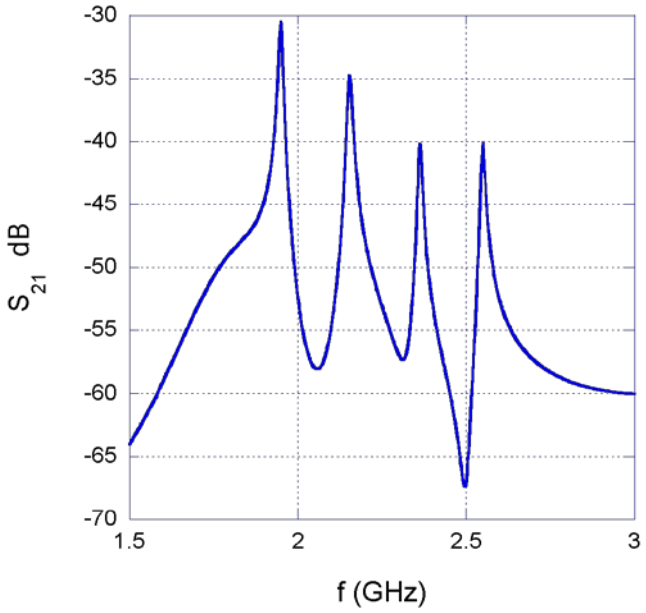

Figure 5. S21 MWO simulation of the designed network.

2.3. Permittivity Detection Through SRR Network

For the purpose of the present work, it is important to be able to evaluate the concrete permittivity starting from the SRR network response. This allows, in the first place, to monitor the concrete status during the curing phase. Furthermore, exploiting the same network embedded in the concrete structure it is possible to implement practically a continuous health monitoring.

Preprints (www.preprints.org) | NOT PEER-REVIEWED | Posted: 18 August 2022 doi:10.20944/preprints202208.0334.v1

All this information can be directly related to the changes in the resonance frequencies of the single SRRs as a result of variations in concrete permittivity. These variations can result from different factors, such as moisture content or air gaps resulting from concrete deterioration. To this purpose, as already highlighted in section 2.1, specific CST parametric simulations have been performed for each SRR changing the permittivity of the surrounding medium (background material) and evaluating the corresponding changes in the scattering matrix.

In this way, calibration curves relating resonance frequency (f_r) to material permittivity (ε) can be obtained. As reported in the literature [13], a second-order polynomial fitting is usually suitable for accurately describing the variation of resonance frequency as a function of permittivity:

$$\varepsilon(f_r) = p_1 f_r^2 + p_2 f_r + p_3 \quad (1)$$

where:

$p_1 = 13;$	$p_2 = -55.5;$	$p_3 = 59.84$	for SRR1
$p_1 = 10;$	$p_2 = -47.68;$	$p_3 = 57.34$	for SRR2
$p_1 = 8.244;$	$p_2 = -43.26;$	$p_3 = 57.27$	for SRR3
$p_1 = 7.067;$	$p_2 = -40.02;$	$p_3 = 57.12$	for SRR4.

In this way, starting from the resonance frequency of the SRR and applying (1), the corresponding permittivity of the material surrounding the sensor can be obtained.

2.3. Wire-like Diffused Sensing Element

The diffused sensing element consists of two cylindrical conductors, parallel to each other and mutually isolated by a plastic covering. This type of sensor, embedded in the system under test (SUT) has one end accessible to perform measurements, allowing a diffused monitoring of SUT and providing information on the entire profile of the structure.

In particular, the microwave reflectometry electromagnetic (EM) measurement technique is used, employed in many monitoring and diagnostic applications [11, 23]. An EM signal propagates through the sensing element located in the SUT. By analyzing the signal that is partially reflected towards the measuring instrument, it is possible to get the wanted information on the SUT, such as for example water content, structural damage and so on.

Figure 6 shows a scheme of the employed sensing element.

The EM signal, usually a step-like signal, propagates along the sensing element and any impedance variation, linked to the changes in the dielectric characteristics of the SUT, generates the partial reflection of the signal. The TDR instrument acquires the reflection coefficient ϱ, that is displayed as a function of time or the traveled apparent distance d_{app} (the distance the signal would travel, in the same time interval, if it was propagating in vacuum); it is given by:

$$\rho = \frac{v_r(t)}{v_{inc}(t)} \quad (2)$$

where, v_r (t) is the amplitude of the reflected signal and v_{inc} (t) is the amplitude of the incident signal.

From the sensing element physical length (L_r) the material effective dielectric constant can be achieved estimating the apparent length (L_a) from the reflectogram:

$$\varepsilon_{app} = 2\left(\frac{L_a}{L_r}\right) \quad (3)$$

 doi:10.20944/preprints202208.0334.v1

considering that the propagation velocity of the signal inside the propagation medium depends on material dielectric properties ε_{app}, and reflects the interaction between the EM signal and the SUT.

The sensing element scheme of Fig. 6 shows the two sensor wires [24].

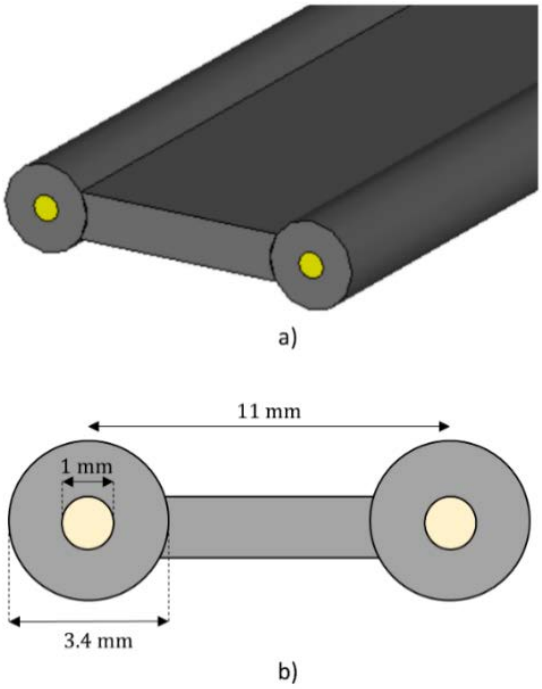

Figure 6. Sensing element perspective view (a) and cross section (b).

3. Experimental Set-Up

The SRR network and the sensing element were embedded in a concrete mix inside a formwork with dimensions 1 m × 0.15 m× 0.15 m. The divider, the combiner and the 4 SRRs have been assembled together, connecting them with flexible coaxial cables. In particular, during the concrete pouring inside the formwork, a first layer of concrete, inside which the diffused sensing element has been embedded, has been deposited in the bottom. Subsequently, a second layer of concrete, housing the SRR network, has been poured in the upper part of the formwork. The two concrete layers have been prepared with a slightly different mixture composition, with a higher cement-to-aggregate ratio in the bottom layer. This different mixture was intentionally created to achieve a lower permittivity around the four SRRs in order to test the effective localization capacity of the variation of the material in the surrounding area. Figure 7 shows the experimental set-up; (a) 3-D view of the four SRRs realizing the distributed network embedded in the concrete beam, (b) a detail of two SRRs inside the formwork during concrete pouring, (c) detail of the SE. This configuration of the network can provide accurate data on four different zones, while the sensing element can supply a diffused monitoring of the system.

A miniaturized vector network analyzer (VNA), namely the nanoVNA (Amsterdam, The Netherlands) is employed for frequency domain measurements. The nanoVNA is a compact miniaturized VNA, with dimensions 15 cm×10 cm×6 cm, it is low-cost and it has 50 kHz–3 GHz frequency range. It has been connected to the four split ring resonators through the power divider and combiner allowing the network S_{21} measurement.

For the TDR measurements a Campbell-Scientific TDR200 (Leicestershire, UK) is used, a low-cost, portable TDR measuring instrument, with dimensions 22 cm×5 cm×11 cm. The TDR200 generates a step-like voltage signal, with a 200 ps rise time, which corresponds to a frequency bandwidth of approximately 1.7 GHz, that propagates through the sensing element embedded in the concrete beam [25, 26].

 doi:10.20944/preprints202208.0334.v1

In this way, measurements were performed over a 28-day period, every day, allowing an accurate monitoring of the concrete curing phase.

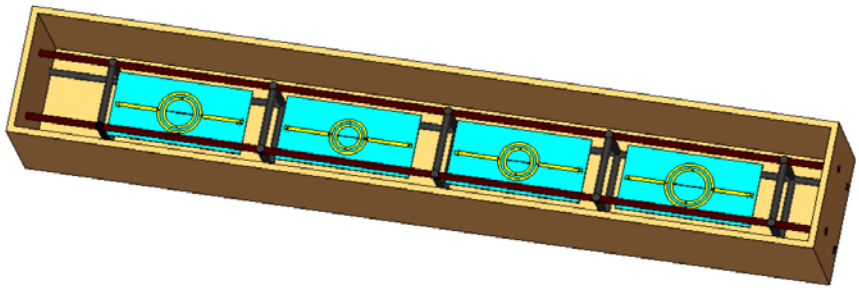

a)

b) c)

Figure 7. Scheme of the experimental setup. (a) 3-D view of the four SRRs embedded in the concrete beam. (b) Picture of the setup showing a detail of the top portion of the beam housing two SRRs during concrete pouring in the formwork. (c) Picture showing a detail of the bottom portion of the beam housing the diffused SE.

4. Results

4.1. Measurements in air

First, the network transmission coefficient measurements have been carried out though the nanoVNA in air, before embedding the network in the concrete beam. Figure 8 shows the measurement results compared with simulations. The experimental curve shows, as expected, large noise levels below -60 dB, due to the intrinsic noise figure of the low-cost miniaturized VNA; however, this noise floor does not affect measurements around the resonance peaks, which occur at much higher levels. It is worth noting here that the MWO circuit model has been improved, in order to obtain the same experimental conditions, by adding to the original circuit schematic the coaxial cables used for connecting the SRRs to the combiner and divider. Due to the presence of the cables, multiple reflections between the SRRs and the combiner/divider networks occur giving rise to additional peaks linked to the resulting stationary waves. These additional peaks are visible on the network transmission coefficient, but they do not affect the detection of the resonance peaks, which are still clearly distinguishable, both in simulation and measurement results. Finally, the observed deviation in amplitude between simulated and experimental data is caused by losses resulting from parasitic effects and non-idealities intrinsically introduced by the experimental setup. However, the results in Fig. 8 clearly show an excellent agreement between experimental and simulated data with reference to resonance frequencies, which are the most significant parameters related to the sensing task.

Preprints (www.preprints.org) | NOT PEER-REVIEWED | Posted: 18 August 2022 doi:10.20944/preprints202208.0334.v1

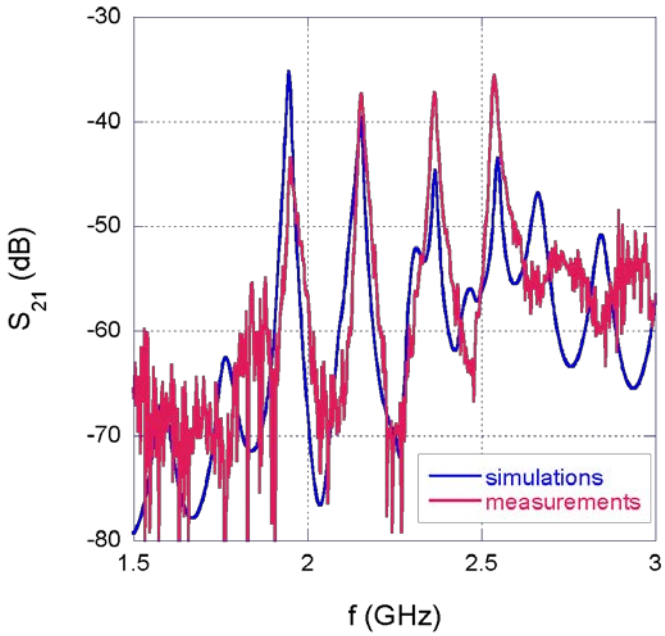

Figure 8. Measured and simulated network transmission coefficient in air.

4.2. Measurements in the concrete beam

After inserting the four SRRs and the sensing element inside the beam during the concrete pouring, measurements on both types of sensors were repeated during the 28 days of hardening of the concrete.

As regards the SRRs, the first day, the presence of a large quantity of water produced a S_{21} which looks like a large bell in which the peaks merged together due to the high losses dramatically decreasing the quality factor. On the second day, however, much of the water has evaporated and the 4 peaks begin to be clearly visible and shift to the right, as expected when permittivity begins to drop.

Figure 9 shows the resonance frequency measured during the curing phase; in particular, the 2nd, 3rd, 4th; 6th, 15th and 28th days are displayed. The resonance frequency of the four SRRs were extrapolated by fitting the data with a Lorentzian curve using MATLAB. In this way, from the resonance frequencies and by applying the calibration curve (1) for the corresponding split ring, the permittivity of the concrete can be extrapolated.

On the two-wire sensing element it is noted that as the days pass, the apparent length decreases (see Fig. 10). In particular, Fig. 10 shows the reflection coefficient as a function of the apparent distance and the related derivative as the days pass.

In order to extrapolate the permittivity of the concrete, the inversion of the measurements in the time domain was carried out using a Matlab algorithm, using a step as an incident pulse. By applying (3) the permittivity can be achieved. Figure 11 shows the obtained results both with the diffused SE and the SRR network.

It is worth noting here that, as already mentioned, the first day the S21 has a bell-shaped trend and the four resonances of the SRR network are not clearly visible; this is the reason why it was not possible to extrapolate permittivity data with the SRR network in Fig. 11 for the first day.

Another important aspect is that the difference in concrete permittivity was deliberately made. In fact, in order to verify if it is possible to notice variations in the surroundings of the planar sensors and therefore to allow precise monitoring, a different mixture of cement was placed around the SRRs in the top layer of the beam structure, with a slightly lower cement-to-aggregate ratio, resulting in a lower permittivity.

Even though the reported experimental results referred only to monitoring of the curing phase, a monitoring of this type will also allow to control the presence of water

Preprints (www.preprints.org) | NOT PEER-REVIEWED | Posted: 18 August 2022 doi:10.20944/preprints202208.0334.v1

inside the beam [28-32], but also to locate any internal cracks in the beam [10, 33] during the entire lifespan of the concrete structure.

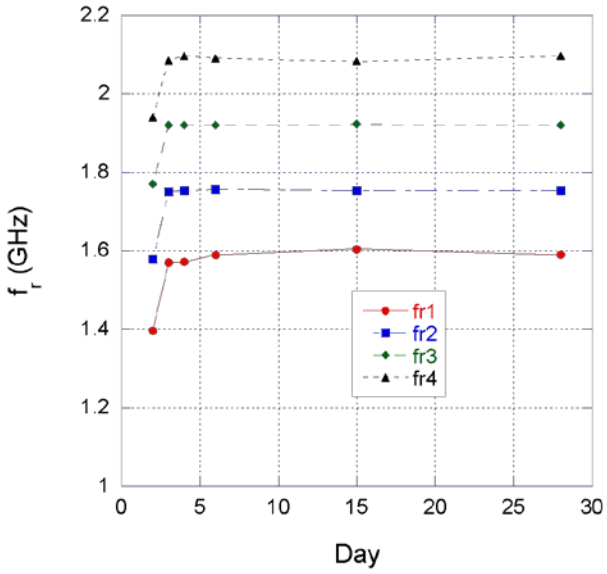

Figure 9. Computed network transmission coefficient resonance frequency during the curing phase.

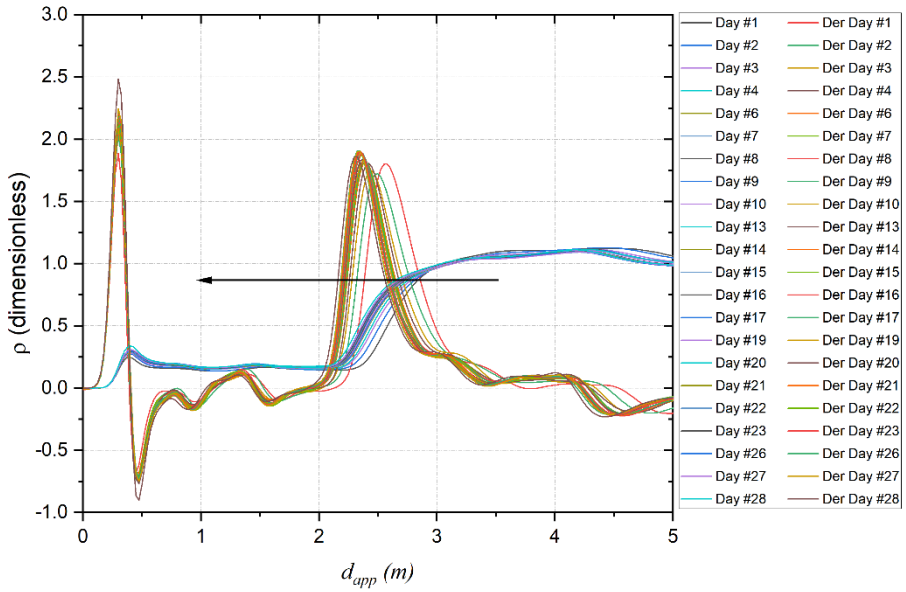

Figure 10. Reflection coefficient as a function of the apparent distance and the related derivative.

Preprints (www.preprints.org) | NOT PEER-REVIEWED | Posted: 18 August 2022 doi:10.20944/preprints202208.0334.v1

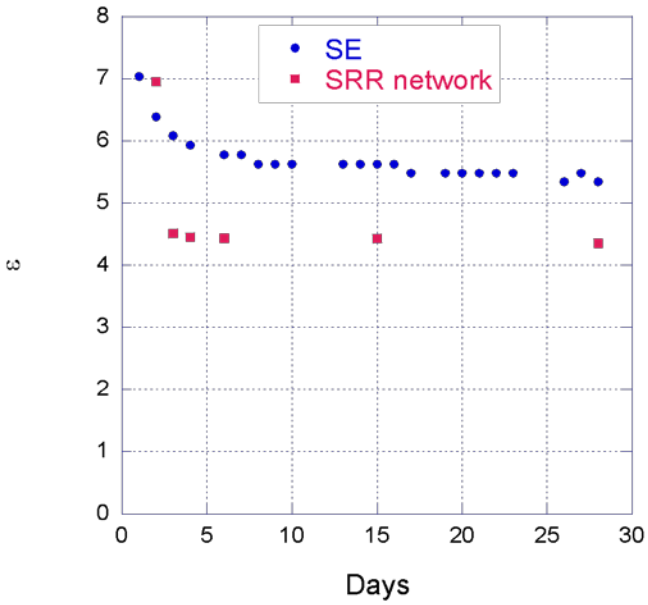

Figure 11. Measured permittivity during the curing of the concrete.

5. Conclusions

In this paper, two sensors for concrete monitoring were presented, a diffuse SE and a network of SRRs for punctual monitoring. The first sensor is able to monitor both the curing phase and possible anomalies arising during the lifespan (water intrusion, detachment of concrete portions, etc.) throughout the concrete structure, which might also be several hundreds of meters long. The second sensor typology, instead, is able to monitor both the presence of water inside the beam and any cracks around the sensor and determine its location thanks to the different working frequencies of resonators; however, the SRR network is only able to cover localized portions of the structure so as to achieve a detailed and sensitive monitoring of possible critical sections of the structure with a distributed localized approach.

The integration of these two structures makes it possible both to monitor concrete during the curing phase, which is very important for the future structural strength of the beam, and to highlight the presence of water that could cause deterioration, especially in cases of dams, bridges and structures that are constantly subjected to an important presence of water.

For future developments it is planned to test the possibility of monitoring the presence of water near one of the SRRs and the localization of artificial cracks, specifically created with mechanical stress in some points of the beam.

Although the present study was limited to a frequency range compatible with portable low-cost instrumentation, a very interesting future development could regard the adoption of miniaturized THz-band sensing structures, thus allowing for a finer distributed sensor network as well as a more efficient detection on micro-cracks occurring during the lifespan of the concrete structure. Such THz structures have been recently proposed in the literature [34- 38].

Author Contributions: Conceptualization, E.P. (Erika Pittella), E.P. (Emanuele Piuzzi) and A.C.; methodology, E.P. (Emanuele Piuzzi); software E.P. (Erika Pittella); validation, R.S., G.M, and A.M; formal analysis, G.M and M.S.; investigation, R.S. and A.M.; resources, A.C. and E.P. (Emanuele Piuzzi); data curation, E.P. (Erika Pittella) and R.S.; writing—original draft preparation, E.P. (Erika Pittella); writing—review and editing, A.C. and E.P. (Emanuele Piuzzi) and R.S.; visualization, E.P. (Emanuele Piuzzi).; supervision, A.C.; project administration, A.C.; funding acquisition, A.C. All authors have read and agreed to the published version of the manuscript.

Acknowledgments: The authors want to thank the Rogers Corporation that provided the dielectric substrate AD255C for the manufacturing of the split ring resonators.

Conflicts of Interest: The authors declare no conflict of interest.

References

[1] J.P. Lynch and K.J. Loh, "A summary review of wireless sensors and sensor networks for structural health monitoring" The Shock and Vibration Digest, vol. 38, no. 2, pp. 91-128, Mar. 2006.

[2] S. Sony, S. Laventure, and A. Sadhu, "A literature review of next-generation smart sensing technology in structural health monitoring," Struct. Control Health Monitoring, vol. 26, e2321, 2019.

[3] A.A. Alzughaibi, A.M. Ibrahim, Y. Na, S. El-Tawil and A. M. Eltawil, "Community-Based Multi-Sensory Structural Health Monitoring System: A Smartphone Accelerometer and Camera Fusion Approach," in IEEE Sensors Journal, vol. 21, no. 18, pp. 20539-20551, 15 Sept.15, 2021, doi: 10.1109/JSEN.2021.3097696.

[4] F. Di Nuzzo, D. Brunelli, T. Polonelli and L. Benini, "Structural Health Monitoring System with Narrowband IoT and MEMS Sensors," in IEEE Sensors Journal, vol. 21, no. 14, pp. 16371-16380, 15 July15, 2021, doi: 10.1109/JSEN.2021.3075093.

[5] N.J. Carino, K.W. Meeks, "Curing of High-Performance Concrete: Phase I study", National Institute of Standards and Technology Report, NISTIR 6505 (2001).

[6] https://www.concretenetwork.com/install-concrete.html

[7] K.H. Teng, P. Kot, M. Muradov, A. Shaw, K. Hashim, M. Gkantou, and A. Al-Shamma'a, "Embedded smart antenna for nondestructive testing and evaluation (NDT&E) of moisture content and deterioration in concrete," Sensors, vol. 19, 2019.

[8] P. Kot, A. Shaw, M. Riley, A. Cotgrave., "The feasibility of using electromagnetic waves in determining membrane failure through concrete," Int. J. Civ. Eng., vol. 15, pp. 355-362, 2017.

[9] M. Gkantou, M. Muradov, G.S. Kamaris, K. Hashim, W. Atherton, and P. Kot, "Novel electromagnetic sensors embedded in reinforced concrete beams for crack detection," Sensors, vol. 19, 2019.

[10] E. Pittella, L. Angrisani, A. Cataldo, E. Piuzzi, F. Fabbrocino, "Embedded Split Ring Resonator Network for Health Monitoring in Concrete Structures", IEEE Instrumentation and Measurement Magazine, 2020, 23(9), pp. 14–20, 9289070.

[11] A. Cataldo, R. Schiavoni, A. Masciullo, G. Cannazza, F. Micelli, E. De Benedetto, "Combined Punctual and Diffused Monitoring of Concrete Structures Based on Dielectric Measurements", Sensors 2021, 21, 4872. https://doi.org/10.3390/s21144872

[12] K. Aydin, I. Bulu, K. Guven, M. Kafesaki, C.M. Soukoulis, and E. Ozbay, "Investigation of magnetic resonances for different split-ring-resonator parameters and designs," New J. Physics, vol. 7, 168, 2005.

[13] R.A. Alahnomi, Z. Zakaria, E. Ruslan, S. Rosmaniza A. Rashid, and A.A. M. Bahar, "High-Q sensor based on symmetrical split ring resonator with spurlines for solids material detection," IEEE Sensors J., vol. 17, no. 9, May, 2017.

[14] R.A. Alahnomi, Z. Zakaria, E. Ruslan, A.A.M. Bahar, and S.R. Ab Rashid, "High sensitive microwave sensor based on symmetrical split ring resonator for material characterization," Microwave and Optical Technology Letters, vol. 58, no. 9, Jun. 2016.

[15] M.S. Boybay and O.M. Ramahi, "Material characterization using complementary split ring resonators," IEEE Trans. Instrum. Meas., vol. 61, no. 11, Nov. 2012.

[16] M.P. Abegaonkar, R.N. Karekar and R.C. Aiyer, "A microwave microstrip ring resonator as a moisture sensor for biomaterials: applications to wheat grains," Meas. Sci. Technol., Jan. 1999.

[17] E. Piuzzi, G. Cannazza, A. Cataldo, E. De Benedetto, L. De Giorgi, F. Frezza, G. Leucci, S. Pisa, E. Pittella, S. Prontera, and F. Timpani, "A comparative assessment of microwave-based methods for moisture content characterization in stone materials," Measurement, vol. 114, pp. 493-500, 2018.

[18] R.A. Alahnomi, Z. Zakaria, E. Ruslan, A.A.M. Bahar, and S.R. Ab Rashid, "A novel microwave sensor with high-Q symmetrical split ring resonator for material properties measurement," J. Teknologi, Aug., 2016.

[19] "CST Studio Suite," 3DS.com, 2019, Dassault Systèmes Deutschland GmbH. Available online: https://www.3ds.com/products-services/simulia/products/cst-studio-suite/.

[20] AD Series Data Sheet - AD250C, AD255C, AD300D and AD350A, available online: https://rogerscorp.com/-/media/project/rogerscorp/documents/advanced-electronics-solutions/english/data-sheets/ad-series-data-sheet---ad250c-ad255c-ad300d-ad350a.pdf

[21] "RF/ Microwave Design," Cadence Microwave Office, RF and Microwave Circuit Design Software, v14.03r. [Online]. Available: https://www.cadence.com/en_US/home/tools/systemanalysis/rf-microwave-design.html.

[22] T. Limer, "Choosing and using resistive power splitters and dividers", Electronic Engineering Times, https://www.edn.com/choosing-and-using-resistive-power-splitters-and-dividers. Published 2008. Accessed May 27, 2022.

[23] E. Piuzzi, E. Pittella, S. Pisa, A. Cataldo, E. De Benedetto, G. Cannazza, "Microwave reflectometric methodologies for water content estimation in stone-made Cultural Heritage materials", Measurement, Volume 118, 2018, Pages 275-281, ISSN 0263-2241, https://doi.org/10.1016/j.measurement.2017.05.069.

[24] A. Cataldo, E. De Benedetto, G. Cannazza, A. Masciullo, N. Giaquinto, G. D'Aucelli, N. Costantino, A. De Leo, M. Miraglia, "Recent advances in the TDR-based leak detection system for pipeline inspection", Measurement 2017, 98, 347–354.

[25] A. Cataldo, E. De Benedetto, G. Cannazza, E. Piuzzi and E. Pittella, "TDR-Based Measurements of Water Content in Construction Materials for In-the-Field Use and Calibration," in IEEE Transactions on Instrumentation and Measurement, vol. 67, no. 5, pp. 1230-1237, May 2018, doi: 10.1109/TIM.2017.2770778.

[26] A. Cataldo, G. Cannazza, E. De Benedetto, N. Giaquinto, "A TDR-based system for the localization of leaks in newly installed, underground pipes made of any material", Meas. Sci. Technol. 23 105010, 2012

[27] E. Piuzzi, A. Cataldo, G. Cannazza, E. De Benedetto, "An Improved Reflectometric Method for Soil Moisture Measurement Exploiting an Innovative Triple-Short Calibration", in IEEE Transactions on Instrumentation and Measurement, vol. 59, no. 10, pp. 2747-2754, Oct. 2010, doi: 10.1109/TIM.2010.2045445.

[28] A. Cataldo, G. Monti; E. De Benedetto; G. Cannazza; L. Tarricone and L. Catarinucci, "Assessment of a TD-Based Method for Characterization of Antennas", in IEEE Transactions on Instrumentation and Measurement, vol. 58, no. 5, pp. 1412-1419, May 2009, doi: 10.1109/TIM.2008.2009199.

[29] N. Giaquinto, G.A. D'Aucelli, E. De Benedetto, G. Cannazza, A. Cataldo, E. Piuzzi, A. Masciullo, "Criteria for Automated Estimation of Time of Flight in TDR Analysis," in IEEE Transactions on Instrumentation and Measurement, vol. 65, no. 5, pp. 1215-1224, May 2016, doi: 10.1109/TIM.2015.2495721.

[30] A. Cataldo, E. De Benedetto, G. Cannazza, E. Piuzzi, N. Giaquinto, "Embedded TDR wire-like sensing elements for monitoring applications, Measurement", Volume 68, 2015, Pages 236-245, ISSN 0263-2241, https://doi.org/10.1016/j.measurement.2015.02.050.

[31] Scarpetta M., Spadavecchia M., Andria G., Ragolia M.A., Giaquinto N., "Analysis of TDR Signals with Convolutional Neural Networks", I2MTC 2021 - International Instrumentation and Measurement Technology Conference, 2021.

[32] Scarpetta M., Spadavecchia M., Adamo F., Ragolia M.A., Giaquinto N., "Detection and characterization of multiple discontinuities in cables with time-domain reflectometry and convolutional neural networks", Sensors, vol. 21, no. 23, 2021.

[33] E. Pittella, E. Piuzzi, "Split Ring Resonator for Complex Permittivity Measurement", 24th IMEKO TC4 International Symposium and 22nd International Workshop on ADC and DAC Modelling and Testing, Pages 85, Palermo, 2020.

[34] R. Feng, B. Ratni, J. Yi, H. Zhang, A. de Lustrac, and S. Nawaz Burokur, "Versatile metasurface platform for electromagnetic wave tailoring", Photonics Research, vol. 9, no. 9, pp. 1650-1659, 2021, https://doi.org/10.1364/PRJ.428853

[35] Q.Yu, Y. N. Zheng, Z. Gu, J. L., Y. C. Liang, L. Z. Li, X. G. Zhang, and W. X. Jiang., "Self-adaptive metasurface platform based on computer vision", Optics Letters, vol. 46, no. 15, pp. 3520-3523, 2021, https://doi.org/10.1364/OL.427527

[36] H. M. Silalahi, Y.-P. Chen, Y.-H. Shih, Y.-S. Chen, X.-Y. Lin, J.-H. Liu, and C.-Y. Huang, "Floating terahertz metamaterials with extremely large refractive index sensitivities", Photonics Research vol. 9, no. 10, pp. 1970-1978, 2021, https://doi.org/10.1364/PRJ.433335

[37] X. Song, W. Yang, K. Qu, X. Bai, K. Chen, Y. Feng, and W. Zhu, "Switchable metasurface for nearly perfect reflection, transmission, and absorption using PIN diodes", Optics Express vol. 29, no. 18, pp. 29320-29328, 2021, https://doi.org/10.1364/OE.436261

[38] R. Xu, X. Xu, B.-R. Yang, X. Gui, Z. Qin, and Y.-S. Lin, "Actively logical modulation of MEMS-based terahertz metamaterial", Photonics Research vol. 9, no. 7, pp. 1409-1415, 2021, https://doi.org/10.1364/PRJ.420876